Extended wavelength infrared photodetectors

Dilip Chauhan
A. G. Unil Perera
Lianhe Li
Li Chen
Suraj P. Khanna
Edmund H. Linfield

Extended wavelength infrared photodetectors

Dilip Chauhan,[a] A. G. Unil Perera,[a,*] Lianhe Li,[b] Li Chen,[b] Suraj P. Khanna,[b] and Edmund H. Linfield[b]
[a]Georgia State University, Department of Physics and Astronomy, Atlanta, Georgia, United States
[b]University of Leeds, School of Electronic and Electrical Engineering, Leeds, United Kingdom

Abstract. Extension of the wavelength threshold of an infrared detector beyond $\lambda_t = hc/\Delta$ is demonstrated, without reducing the minimum energy gap (Δ) of the material. Specifically, a photodetector designed with $\Delta = 0.40$ eV, and a corresponding $\lambda_t = 3.1$ μm, was shown to have an extended threshold of $\sim$45 μm at 5.3 K, at zero bias. Under negative and positive applied bias, this range was further extended to $\sim$60 and $\sim$68 μm, respectively, with the photoresponse becoming stronger at increased biases, but the spectral threshold remained relatively constant. The observed wavelength extension arises from an offset between the two potential barriers in the device. Without the offset, another detector with $\Delta = 0.30$ eV showed a photoresponse with the expected wavelength threshold of $\sim$4 μm. © *2017 Society of Photo-Optical Instrumentation Engineers (SPIE)* [DOI: 10.1117/1.OE.56.9.091605]

1 Introduction

The spectral photoresponse range of semiconductor infrared (IR) detectors is conventionally determined by the relationship $\lambda_t = hc/\Delta$, where λ_t is the wavelength threshold of the photoresponse and Δ is the minimum energy gap for the photoexcitation, also known as the activation energy.[1] In p-type GaAs/Al$_x$Ga$_{1-x}$As heterojunction IR detectors, absorption of IR radiation leads to hole transitions from the light-hole/heavy-hole bands to the split-off band, and from the heavy-hole to light-hole bands. Free-carrier absorption is also possible, resulting in photoexcitation in the heavy-hole/heavy-hole bands. The latter process is weaker at shorter wavelengths but increases with the wavelength[2] as λ^2. Thus, a p-GaAs layer absorbs a broad IR spectrum. However, the limit of the spectral photoresponse of p-GaAs/Al$_x$Ga$_{1-x}$As detectors is normally determined by the activation energy[3] (Δ), defined as the interfacial energy gap at the emitter (absorber)/barrier interface; that is, the difference between the Fermi level in the p-GaAs emitter and the potential barrier in the Al$_x$Ga$_{1-x}$As layer. Even though Δ can be adjusted to cover the mid-IR to far-IR spectral ranges,[4,5] lowering the value of Δ always leads to an increased dark current and an increase in the related noise levels. Recently, it was reported[6] that the wavelength threshold can be dramatically extended beyond the expected value of λ_t. A p-GaAs/Al$_x$Ga$_{1-x}$As-based heterostructure was tested, where Al$_x$Ga$_{1-x}$As barriers on two sides of a p-GaAs emitter had different barrier heights, introducing an offset (δE) $\sim$0.10 eV. It was proposed that the photoexcited high energy carriers, also known as hot carriers, injected from the high energy barrier side interact with the cold carriers at the emitter, leading to a transient energy redistribution, with the cold carriers elevated to higher energy states.[7] With the Fermi level elevated, the effective Δ is reduced; therefore, the photoresponse of the detector is extended to a longer wavelength range. Based on this mechanism, a detector designed with a Δ corresponding to mid-IR ($\sim$3.1 μm) wavelengths showed a very long wavelength IR (VLWIR) photoresponse,[6] up to $\sim$55 μm. However, the reported extended wavelength photoresponse was principally limited to a narrow range of negative applied bias. Optimization of the detector operation and performance requires the ability to use a broader range of applied biases. Here, we demonstrate a designed detector with $\delta E \sim 0.19$ eV and designed $\Delta \sim 0.40$ eV, showing photoresponse up to $\sim$45 μm at zero bias and $\sim$60 and $\sim$68 μm in negative and positive bias regimes, respectively.

2 Device Design and Experiments

Four IR detectors were studied: LH1002, SP1001, SP1007, and 15SP3, as summarized in Table 1. Each is a p-GaAs/Al$_x$Ga$_{1-x}$As heterostructure, grown by molecular beam epitaxy on a semi-insulating GaAs substrate. The valence band alignment of the heterostructures at zero bias is shown schematically in Fig. 1. The active region in each detector is sandwiched between p-type doped GaAs contact layers, with bottom and top contact thicknesses of 0.5 and 0.2 μm, respectively. The active layers consist of an Al$_x$Ga$_{1-x}$As barrier, followed by a p-GaAs emitter, and then by another Al$_x$Ga$_{1-x}$As barrier. The emitter and the top and bottom contact layers are doped at 1×10^{19} cm^{-3}, and the thicknesses of the emitters in all detectors are sufficiently large to have a bulk-like distribution of energy states. Sample LH1002, the reference detector used in this study, consists of a 20-nm emitter and constant Al$_{0.57}$Ga$_{0.43}$As barriers (60 nm), so that there is no energy offset between the two barriers. Sample SP1001 consists of an 80 nm emitter, a constant Al$_{0.75}$Ga$_{0.25}$As barrier (80 nm) at the bottom, and a second constant Al$_{0.57}$Ga$_{0.43}$As barrier (400 nm) at the top, so that there is an energy offset (δE) of $\sim$0.10 eV. Sample SP1007 is similar to SP1001, except for the top Al$_x$Ga$_{1-x}$As barrier, which is graded by tuning the Al mole fraction from

---

Table 1 Summary of sample parameters and wavelength thresholds. All emitters and the top and bottom contacts (p-GaAs) are doped at 1×10^{19} cm^{-3}.

| | Δ (eV) (designed) | Energy offset (δE) (eV) | Al mole fraction | | | w_e (nm) | w_1 (nm) | w_2 (nm) | Wavelength threshold (λ_t) at 5.3 K |
			x_1	x_2	$x_3 = x_4$				
LH1002	0.30	None	0.57	0.57	0.57	20	20	60	~4 μm (−0.2 V)
SP1001	0.40	0.10	0.75	0.75	0.57	80	80	400	>36 μm
SP1007	0.40	0.10	0.45	0.75	0.57	80	80	400	~55 μm (−0.06 V) (Ref. 6)
15SP3	0.40	0.19	0.45	0.75	0.39	80	80	400	~60 μm (−1 V), ~68 μm (3 V), ~45 μm (0 V)
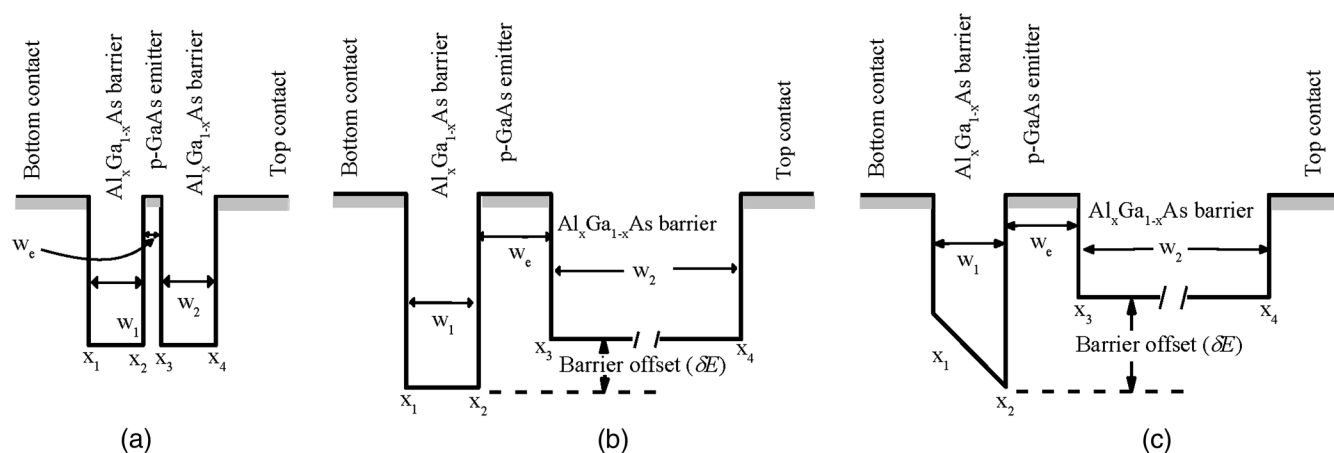
Fig. 1 Schematic diagrams of the valence band alignment of the detectors under equilibrium: (a) LH1002 consists of an emitter (20 nm) and two Al$_{0.57}$Ga$_{0.43}$As barriers (60 nm), with no energy offset between the barriers. (b) SP1001 consists of an emitter (80 nm), an 80 nm Al$_{0.75}$Ga$_{0.25}$As barrier at the bottom, and a 400 nm Al$_{0.57}$Ga$_{0.43}$As barrier at the top, so that there is an energy offset (δE) of ~0.10 eV between the barriers. (c) In SP1007, the Al$_x$Ga$_{1-x}$As barrier (80 nm) at the bottom is graded by tuning the Al mole fraction from $x_1 = 0.45$ at the bottom to $x_2 = 0.75$ at the top, while it utilizes a constant upper Al$_{0.57}$Ga$_{0.43}$As barrier (400 nm). There is an energy offset ($\delta E \sim 0.10$ eV) between the barriers. Sample 15SP3 utilized a constant Al$_{0.39}$Ga$_{0.61}$As barrier at the top, with other parameters kept the same as SP1007, so that the energy offset is larger ($\delta E \sim 0.19$ eV). The emitters are thick enough to have a bulk-like distribution of energy states. For all samples, the emitter and the top and bottom contacts are p-type doped at 1×10^{19} cm^{-3}.

$x_1 = 0.45$ at the bottom to $x_2 = 0.75$ at the top. Finally, sample 15SP3 utilizes similar parameters to SP1007, but the energy offset is larger ($\delta E \sim 0.19$ eV) due to a lower Al mole fraction ($x_3 = 0.39$) in the constant barrier at the top. The details of the sample parameters and spectral photoresponse thresholds are summarized in Table 1. Mesas were fabricated by conventional photolithography and wet etching, followed by Ti/Pt/Au metallization to form contact electrodes. Each mesa has an electrically active area of 400×400 μm^2. The top contact layer (p-GaAs) was partially etched to form an optical window of ~260×260 μm^2 for normal incidence optical illumination of the detector.

Current–voltage characteristics were measured using a Keithley 2400 source meter. A positive bias on the device refers to a positive voltage connected to the top contact, with the bottom contact grounded. Similarly, a negative bias refers to the positive voltage connected to the bottom contact, with the top contact grounded. Spectral photoresponse was measured using a Fourier transform infrared

spectrometer and calibrated using a commercial Si composite bolometer to measure the background intensity.
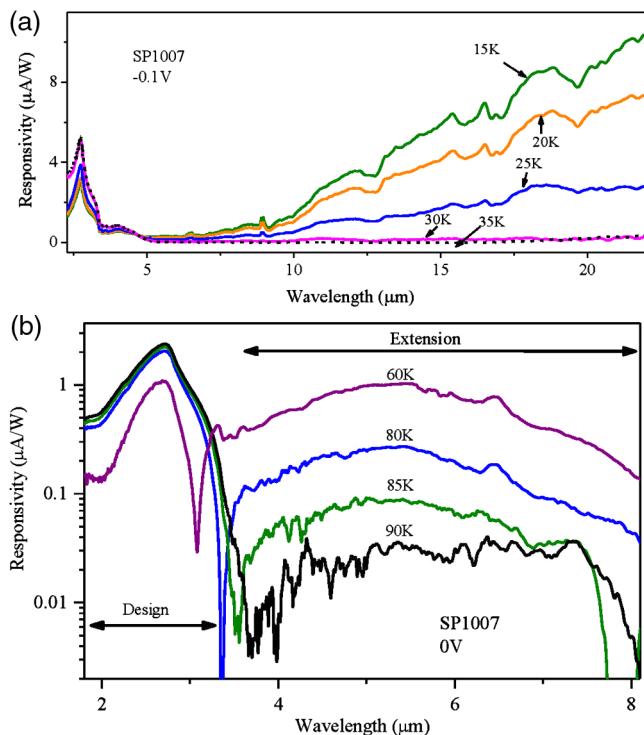
3 Results and Discussion

A comparison of the photoresponse, measured at 5.3 K, for structures LH1002, SP1001, and SP1007 is shown in Fig. 2. LH1002, without an energy barrier offset, showed a photoresponse up to ~4 μm, closely agreeing with the designed value of $\Delta \sim 0.30$ eV. However, both SP1001 and SP1007 showed an extended wavelength photoresponse into the VLWIR range, owing to the energy band offset ($\delta E \sim 0.10$ eV), which led to the energies of holes on the injection side being higher than those on the collection side.[8] An energy redistribution then takes place as the injected hot holes transfer energy to the cold holes in the emitter. This transient process results in an elevated Fermi level in the emitter, thereby reducing Δ and leading to the photoresponse extension. A detailed study of the VLWIR
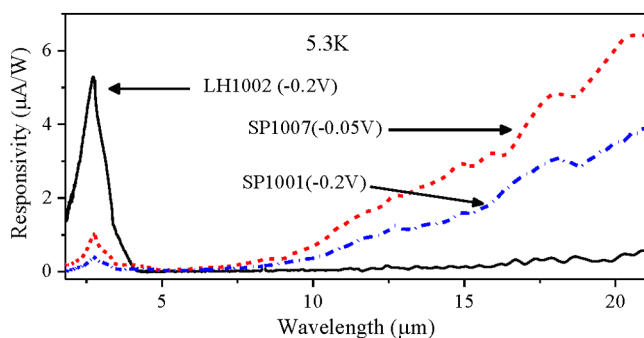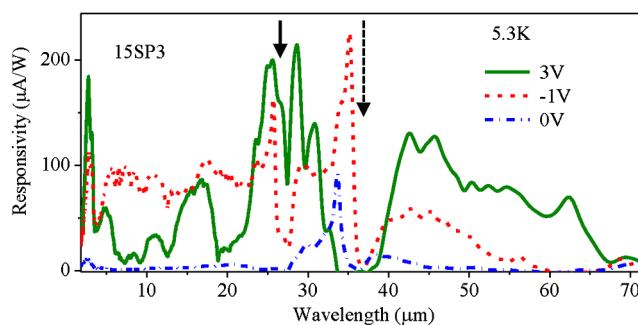
Fig. 2 A comparison of the spectral photoresponse of the detectors LH1002, SP1001, and SP1007 at 5.3 K: LH1002, without a barrier offset, does not show an extended wavelength photoresponse. Owing to an energy offset ($\delta E \sim 0.10$ eV), both SP1001 and SP1007 show an extended wavelength photoresponse. SP1007, the structure with a graded barrier, shows a stronger extended response.

Fig. 4 Spectral photoresponse of the detector at 5.3 K: up to ~60 μm under negative bias, up to ~68 μm under positive bias, and up to ~45 μm at zero bias. For comparison, the designed value of Δ should give a threshold wavelength of only ~3.1 μm. Solid and dashed arrows mark features associated with the AlAs-like and GaAs-like phonons, respectively. In comparison to the negative bias data, the AlAs-like phonon feature is narrowed under positive bias, while the GaAs-like phonon feature is widened.

photoresponse in SP1007, with varying degrees of hot hole injection, was previously reported in Ref. 6.

As the temperature was increased from 5.3 K, the VLWIR photoresponse of SP1007 gradually decreased and vanished at 35 K, as shown in Fig. 3(a). A possible reason for this may be that the hot–cold carrier energy transfer becomes less efficient with increasing temperature as the carrier–carrier energy transfer can be affected by other processes, such as carrier-ionized dopant scattering, causing a reduced carrier–carrier scattering rate. It is also possible that the lifetime of the hot carriers is reduced with increasing temperature,

Fig. 3 (a) Effect of temperature on the VLWIR photoresponse of sample SP1007, showing that the extended wavelength photoresponse gradually decreases above 5.3 K and vanishes at 35 K. (b) At higher temperatures (up to 90 K), wavelength extension was observed up to ~8 μm, which is beyond the designed limit of 3.1 μm. (Reprinted with permission from Ref. 10. Copyright 2016, SPIE Digital Library).

making the energy transfer process less efficient. Even though the VLWIR photoresponse was limited to temperatures below 35 K, a photoresponse beyond Δ was observed up to 90 K, as shown in Fig. 3(b). The photoresponse measured at zero bias, showed a wavelength extension up to ~8 μm, compared with the wavelength threshold of ~3.1 μm expected from the design ($\Delta \sim 0.40$ eV). As the holes in the emitter absorb IR radiation and gain extra momentum, carrier transport can occur toward both top and bottom contacts, giving rise to forward and reverse photocurrents. The process of photoexcited carriers escaping over the emitter–barrier interface is called internal photoemission,[9] and the photoemission efficiency is proportional to $(\varepsilon - \Delta)$, where ε is the energy of the photoexcited holes and Δ is the interfacial energy gap. Therefore, the net photocurrent is determined by the difference of the photoemission efficiencies in the opposite directions.

As reported previously for sample SP1007, the wavelength extension to the VLWIR range was principally observed over a small range of negative bias.[6] Also, based on a study of the spectral weight of the photocurrent as a function of bias, it was observed that only negative bias conditions gave an optimum extended wavelength photoresponse. However, by modifying the detector to give a higher energy offset ($\delta E \sim 0.19$ eV) in sample 15SP3, an improved operational bias range was obtained. Specifically, an extended photoresponse into the VLWIR range was observed at both positive and negative applied biases (Fig. 4), with the spectral range at positive biases being extended to longer wavelengths (~68 μm) than that at negative biases (~60 μm). Additionally, an extended photoresponse was observed at zero bias up to ~45 μm. Hence, by using in 15SP3 a structure with higher δE, restrictions on the bias direction and range were removed.

Under a negative bias, the VLWIR photoresponse can be understood in terms of hot–cold carrier energy transfer, due to hot carriers injected from the bottom contact to the emitter leading to a change in the energy redistribution of the carriers in the emitter itself. The sharp peaks observed in the photoresponse near 25.5 and 35.6 μm are consistent with previously observed peaks due to strong plasmon–phonon coupling modes.[6] Moreover, under negative applied bias, the features associated with AlAs-like and GaAs-like
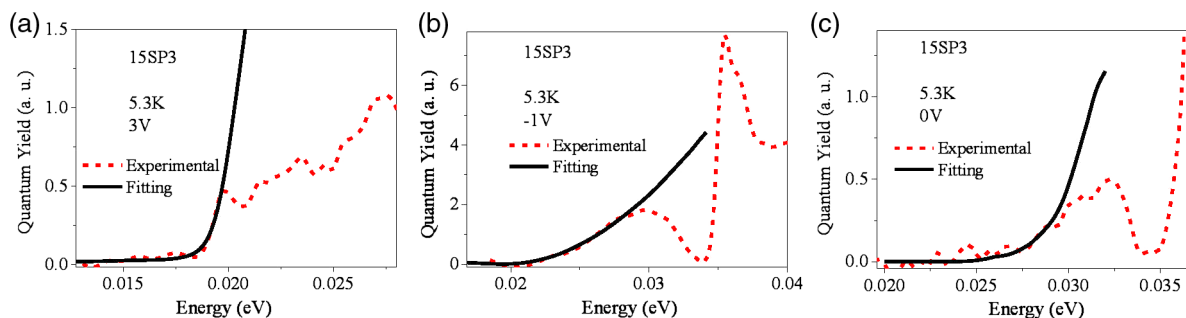
Fig. 5 TDIPS fitting of the experimentally measured photoresponse of 15SP3 to obtain the threshold energy of the spectral photoresponse 5.3 K: (a) at 3 V, (b) at −1 V, (c) at 0 V. Solid and dashed lines represent fitted and experimental curves, respectively.

phonons (in Fig. 4, these are marked by solid and dashed arrows, respectively) are similar to those observed previously.[6] However, under positive bias, the AlAs-like phonon feature becomes narrow, while the GaAs-like phonon feature is widened, although the cause of this difference is unclear at the moment.

Under a positive bias, hot carriers are injected from the top contact, that is, over the lower energy barrier. The escape of photoexcited carriers toward the bottom contact would, however, be less likely due to the high energy of the graded barrier. As the applied positive bias increases, however, the graded barrier assumes a sharp triangular shape, and a barrier lowering occurs due to image force effect.[11] As a result, carriers escape and collection may be enhanced and reinforced due to the tunneling near the tip of the graded barrier, explaining the observed VLWIR photoresponse under a positive bias.

At zero bias, net injection of photoexcited carriers from either the top or bottom contacts will be relatively weak. Nevertheless, a photoresponse is observed up to ∼45 μm. More analytical studies are important to unravel the physical processes leading to this extended wavelength photoresponse and to further interpret the differences in spectra under positive and negative biases.

Arrhenius plots were obtained from the temperature-dependent current–voltage characteristics. The activation energy (Fig. 6) of the detector obtained from the Arrhenius plots indicates that the interfacial energy gap near zero bias agrees closely with the designed value of $\Delta \sim 0.4$ eV. Due to the asymmetry of the device structure, barrier lowering due to the image force effect is different between positive and negative applied biases. To compare the bias-dependent activation energy with the spectral threshold, the photoresponse was also measured at 77 K. The energy corresponding to the spectral threshold of the photoresponse was then determined using the temperature-dependent internal photoemission spectroscopy (TDIPS) method.[9] In this method, the quantum yield $[Y(h\nu) \sim (h\nu - \Delta)^2]$ of the photoresponse is fitted in the near-threshold region (Fig. 5) to obtain a value of Δ as a fitting parameter. A comparison (Fig. 6) shows that the spectral thresholds of the photoresponse agree closely with the activation energy in the bias ranges of −0.4 to −1 V, and 3 to 4.5 V. In the bias range of −0.4 to 3 V, however, the spectral threshold deviates from the activation energy and is extended to longer wavelengths. Furthermore, the spectral threshold of the photoresponse measured at 5.3 K is distinctly different from the activation energy in
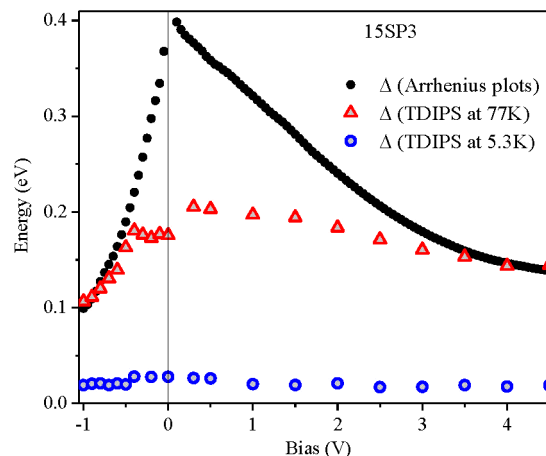
Fig. 6 A comparison of the activation energies obtained from Arrhenius plots of the temperature-dependent dark currents, with the threshold energy of the photoresponse obtained from the TDIPS (Ref. 9). At 77 K, these values agree closely in the bias ranges of −0.5 to −1 V, and 3 to 4.5 V. Between −0.4 and 3 V, however, the energy values obtained from the TDIPS method deviate significantly from those obtained from Arrhenius methods, indicating an extended wavelength photoresponse. At 5.3 K, the energy values obtained from TDIPS are dramatically smaller in the entire bias range of −1 to 4.5 V, indicating a threshold extension throughout the bias range.

the entire bias range from −1 to 4.5 V. The spectral threshold at zero bias is ∼45 μm (0.028 eV), while it is ∼60 μm (0.021 eV) and ∼68 μm (0.018 eV) at −1 and 3 V, respectively. Moreover, the spectral thresholds remain relatively constant in the negative and positive biases. This is an indication that the wavelength extension mechanism is mostly independent of the applied bias and, hence, the image-force effect. However, the photoresponse becomes stronger at increased applied biases, indicating that the collection efficiency improves with the increased bias.

4 Conclusions

We demonstrated a p-GaAs/Al$_x$Ga$_{1-x}$As heterostructures-based IR detector with an energy offset (δE) between the barriers. The detector showed a photoresponse that was dramatically larger than the conventional limit of the interfacial energy gap (Δ) of the heterostructure. Without the offset, an equivalent photodetector showed the expected threshold of ∼4 μm closely agreeing with the designed value of $\Delta \sim 0.30$ eV. The detector with $\Delta \sim 0.4$ eV (3.1 μm) and $\delta E \sim 0.19$ eV showed a photoresponse up to ∼45 μm at

zero bias, at 5.3 K. Under negative and positive biases, a photoresponse was observed up to ∼60 and 68 μm, respectively. As opposed to previously reported results on wavelength extension, which were only observed over a small range of negative biases, the results in this study clearly indicate that extended wavelength detectors can be designed to operate over a wide range of biases, thereby easing optimization of the detector performance, including operating temperature.

References

1. S. M. Sze and K. K. Ng, *Physics of Semiconductor Devices*, p. 644, John Wiley & Sons, New Jersey (2007).
2. A. L. Korotkov et al., "Free-carrier absorption in Be- and C-doped GaAs epilayers and far infrared detector applications," *J. Appl. Phys.* **89**(6), 3295–3300 (2001).
3. D. G. Esaev et al., "Design and optimization of GaAs/AlGaAs heterojunction infrared detectors," *J. Appl. Phys.* **96**(8), 4588–4597 (2004).
4. M. B. M. Rinzan et al., "Terahertz absorption in AlGaAs films and detection using heterojunctions," *Infrared Phys. Technol.* **47**(1–2), 188–194 (2005).
5. S. G. Matsik et al., "Cutoff tailor ability of heterojunction terahertz detectors," *Appl. Phys. Lett.* **82**(1), 139–141 (2003).
6. Y. F. Lao et al., "Tunable hot-carrier photodetection beyond the bandgap spectral limit," *Nat. Photonics* **8**(5), 412–418 (2014).
7. F. Capasso, "Band-gap engineering: from physics and materials to new semiconductor devices," *Science* **235**(4785), 172–176 (1987).
8. T. Elsaesser et al., "Relaxation processes of hot holes in Ge and GaAs investigated by ultrafast infrared spectroscopy," *Semicond. Sci. Technol.* **9**(5S), 689–693 (1994).
9. Y. F Lao and A. G. U. Perera, "Temperature-dependent internal-photoemission probe for band parameters," *Phys. Rev. B* **86**(19), 195315 (2012).
10. A. G. U. Perera et al., "Infrared photodetectors with wavelength extension beyond the spectral limit," *Proc. SPIE* **9844**, 98440X (2016).
11. A. G. U. Perera, H. X. Yuan, and M. H. Francombe, "Homojunction internal photoemission far-infrared detectors: photoresponse performance analysis," *J. Appl. Phys.* **77**(2), 915–924 (1995).

Biographies for the authors are not available.